Post-print: Langmans, J., Desta, T., Alderweireldt, L., Roels, S. (2016). Field study on the air change rate behind residential rainscreen cladding systems: a parameter analysis. *Building and Environment, 95* (1), 1-12.

Field study on the air change rate behind residential rainscreen cladding systems: a parameter analysis

Jelle Langmans[a]*, Tadiwos Z. Desta[b], Lieven Alderweireldt[b], Staf Roels[a]

[a]Department of Civil Engineering, Building Physics Section, University of Leuven
Kasteelpark Arenberg 40 - bus 02447, BE-3001 Heverlee, Belgium
[b] Redco nv, Kuiermansstraat 1, B-1880 Kapelle-op-den-Bos, Belgium

** Corresponding author. Tel: +32 16 321348; fax: + 32 16 32 19 80.*
E-mail address: jelle.langmans@bwk.kuleuven.be (J. Langmans)

Abstract

The article at hand presents the results of an extensive field study in which the air change rate behind rainscreen claddings has been measured. In total eight different full-scale test walls have been tested. The main parameter varations are: 1) the cladding system (brick veneer and sidings), 2) orientation (South-West and North-East) and 3) area of ventilation openings. To increase the reliablity of the results four measuring techniques to determine the air change rate have been applied. The accuray and applicability of these methods have been discussed in a previous paper. The current article focusses on the impact of the three abovementioned parameter variations on the overall air change rate. Moreover their effect on the hygrothermal conditions in the cavities will be outlined. The results show that the cavity ventilation for brick veneer (1-10 ACH) is two order of magnitude lower than behind sidings (100-1000ACH). This difference also reflects on the drying potential of both systems. The vapour content behind the sidings follows closely the outer climate. In contrast the vapour pressure behind brick veneer can be significantly higher than the outer climate which is induced by its moisture buffer capacity and its low ventilation rate.

Keywords: cavity ventilation, field tests, hygrothermal, airflow, brick veneer, sidings

NOMENCLATURE

Roman

ACH	Air change rate	(1/h)
C_p	Pressure coefficient	(-)
I	Irradiance	(W/m²)
n	Flow exponent	(-)
h	Height	(m)
Q	Air flow rate	(m³/s)
T	Temperature	(K)
U	Velocity	(m/s)
P	Pressure	(Pa)
RH	Relative humidity	(%)

Abbreviations

OHJ	Open head joint
HAM	Heat, Air and Moisture
SW	South West
NE	North East

Subscripts

av	average (in time)
b	buoyancy
ex	exterior
hor	horizontal
c	cavity
m	average (in space)
out	outdoor
v	vapour

1. Introduction

Ventilated wall claddings are widely applied to protect the building envelope from rain water ingression [1]. Rainscreen cladding serves as a drainage layer and a capillary break between the outer climate and the inner structural elements. In addition, cavity ventilation behind the cladding system promotes the evacuation of trapped moisture by means of convection. In contrast to the straightforward process of gravity-driven drainage of rain water to avoid water penetration, the convective removal of moisture is a complex process influenced by many parameters (e.g. ventilation rate, the material properties of the system, the indoor and climate conditions and the configuration of the cavity). A number of experimental studies have been investigating cavity ventilation behind rainscreen cladding for specific configurations. For example, a Danish study by Gudum [2] applied a tracergas technique based on the injection of nitrous oxide to study the ventilation rate behind a plexiglass cladding layer. A similar method, but based on carbon dioxide tracer gas, has been used in New-Zealand by Basset and McNeil [3] to study the ventilation rate behind brick veneer. TenWolde et al. [4], on the other hand, established a methodology to determine the ventilation rate based on the measured air pressure differences across the rainscreen cladding. In addition, several scholars measured cavity ventilation by using anemometry methods [e.g. 2,5]. A thorough study on cavity ventilation behind rendered cladding panels with anemometry is documented by Falk and Sandin [5]. The air change rate in their experiment was studied with an omnidirectional anemometer in the middle of the cavity. Falk and Sandin described that the air flow direction in these cavities changes with a high frequency induced by unstable wind pressures. These changing flow conditions could not be quantified with the applied omnidirectional anemometer. As a remedy theses authors developed a method to compensate for these changing flow conditions in the calculation of the air change rate. Their method is based on calibration periods with known flow direction in the cavity (periods with low wind velocities and high levels of solar radiations resulting in upward flow). Also Labat et al. [6] applied anemometry to measure the ventilation rate behind a wooden cladding. Their focus was however limited to solar dominated periods avoiding the difficulties of changing air flow direction related to dynamic wind effects. Sandin [7] measured - in addition to the electronic measuring techniques - the air change rate with smoke visualisation on brick veneer cladding.

Though this method revealed interesting insights in the air flow pattern behind brick veneer, it was difficult to derive accurate air change rate levels for this type of cladding system.

The above documented field measurements correspond to a wide range of methods to determine cavity ventilation levels. However, only few of these works verified the accuracy and applicability of the proposed techniques. Moreover, the tests have been conducted for a wide range of cladding systems and materials impeding a straightforward comparison between the different documented methods.

In addition to the remaining questions regarding the effectiveness of cavity ventilation, its implementation in building component HAM-models remains a topic of debate. Today several cavity ventilation models are implemented in HAM-tools ranging from 1) the omission of ventilation effects [8], 2) effective cladding diffusion permeance [9,10], 3) neglecting the cladding system [11], 4) the application of a constant air change rate [12,13], 5) simplified coupled implementations [14] and 6) fully-coupled models [15]. Yet the impact of these ventilation models on the obtained outcome – which can be large - is hardly validated with experimental data.

In order to study the impact of cladding design decisions on its ventilation rate and subsequent its hygrothermal consequences, a full scale test setup has been built in Leuven, Belgium. In total eight test walls have been constructed. The walls are applied to investigate the accuracy of the existing measuring methods and to verify the impact of several design options on the overall cavity ventilation and hygrothermal conditions. In a previous article the accuracy and applicability of the applied experimental measuring techniques are documented for *in-situ* test walls with brick veneer and sidings systems [16]. The results illustrated that the methods based on pressure differential and anemometry have the widest applicability and highest accuracy. This study further revealed that for low ventilation rates (<10 ACH) the anemometer measurements were biased by local buoyancy effects induced by thermal bridging effects of the sensors. As a consequence the study advises to apply the method based on measuring the pressure differential instead of anemometry for cladding with low ventilation rate such as brick veneer. For wall cladding with higher ventilation rates, such as sidings or (rendered) façade panels both methods perform equally.

The aim of the present work is to study the impact of the cladding configuration on its overall air change rate. The test setup applied in [16] has been used here to investigate the influence of following parameters:

- Cladding system: brick veneer and fibre cement sidings
- Orientation
- Ventilation openings

Moreover the present work documents the hygrothermal conditions in the cavity for the different configurations.

First, the experimental test-setup will be briefly outlined focusing on the measuring techniques applied in the present paper. Second, the theoretical driven potentials for cavity ventilation will be discussed and verified with the measured data. Thereafter the impact of the three design parameters on the overall cavity ventilation rate will be examined. In addition the influence of these parameters on the hygrothermal conditions within the cavity will be discussed in the final section of this paper. This will result in recommendations to include cavity ventilation in building component HAM-models.

2. Experimental test-setup and measuring methods

2.1. Global test wall configuration

Field measurements on cavity ventilation are performed at the VLIET-test building of KU Leuven, Belgium. This test building has measuring sections, oriented to the Northeast and the Southwest. In Belgium, Southwest is the direction of prevailing winds, wind-driven rains and solar irradiation. Northeast oriented façades, on the other hand, hardly receive any sun or rain. The building is equipped with a weather station positioned at the ridge of the sloped roofs module and a weather station in the nearby open field. Both stations register the outside climate conditions on a minutely basis (humidity, temperature, wind direction and speed, global solar irradiation, horizontal rainfall). More information on the building's geometry, location and orientation can be found in [17-18].

Eight individual walls have been studied in this test building. Figure 1 illustrates the configuration of the test walls which are installed on both the North East oriented and South West oriented test bays of the building. For both orientations two separated walls are finished with brick veneer cladding and two are executed with fibre cement sidings. The test walls have a height of 2.7 m and a width of 0.9 m. For all the test walls a cavity depth of 4 cm was applied. In walls A, brick veneer with a thickness of 9 cm is used in which a grid system is provided at the bottom and top allowing to change the number of open head joints. The number of open head joints in this system could be varied from 0 to 30 openings per meter with the configuration of each opening being 3.5x1.5x9 cm^3. For the test walls B, 1cm thick, white coloured, and hydrophobised fibre cement sidings are applied. The test walls have a ventilation opening of 4 cm at the top. The bottom opening is closed with a perforated metal sheet to protect the wall from vermin. The air permeability of both cladding systems are documented in [16]. To minimise the heat and mass transport from the interior (19°C / 50%RH) and between neighbouring wall cavities, each section was carefully sealed at the inside. In addition an airtight and vapour tight XPS-layer of 5 cm was applied between the test walls. Also the borders of the cladding systems have been precisely caulked with weather resistant silicone into the test frame to avoid air leakages at the edges and to

promote two-dimensional conditions in the ventilation cavities.

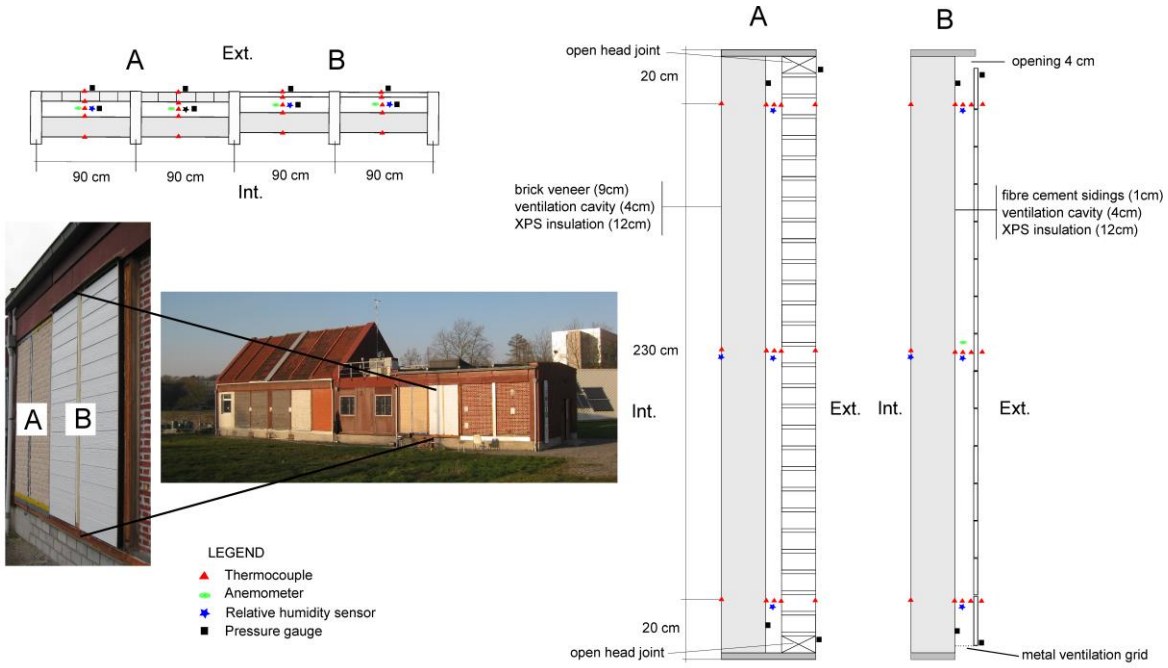

Figure 1: Southwest façade of the VLIET test building with (A) brick veneer test wall and (B) test wall with fibre cement sidings.

2.2. Parameter variations

Table 1 shows an overview of the different parameters which have been varied during the experiment which ran from January 2014 to September 2014. The three main parameters are: 1) cladding system (brick vs. sidings), 2) the orientation (Southwest vs. Northeast) and 3) the area of the ventilation in- and outlet. For the latter, a grid installed at the top and bottom of the brick veneer layer makes it possible to change the number of open head joints (see section 2.1). The discussion in the present article is limited to the periods in which the number of open head joints was 0, 1 or 2 at both top and bottom. For the walls with sidings two configurations have been tested: 1) open at top and bottom and 2) open at bottom and closed at top with airtight tape.

WALL NAME	CLADDING	ORIENTATION	30/01-07/02	07/02 - 06/03	07/03-01/09
W4A	BRICK	NORTH-EAST	OHJ_{TOP}=1, OHJ_{BOTTOM}=1	OHJ_{TOP}=2, OHJ_{BOTTOM}=2	OHJ_{TOP}=2, OHJ_{BOTTOM}=2
W4B			-	OHJ_{TOP}=1, OHJ_{BOTTOM}=1	OHJ_{TOP}=0, OHJ_{BOTTOM}=0
W24A	BRICK	SOUTH-WEST	OHJ_{TOP}=1, OHJ_{BOTTOM}=1	OHJ_{TOP}=2, OHJ_{BOTTOM}=2	OHJ_{TOP}=2, OHJ_{BOTTOM}=2
W24B			OHJ_{TOP}=1, OHJ_{BOTTOM}=1	OHJ_{TOP}=1, OHJ_{BOTTOM}=1	OHJ_{TOP}=0, OHJ_{BOTTOM}=0
W3A	SIDINGS	NORTH-EAST	T=OPEN, B=OPEN	T=OPEN, B=OPEN	T=OPEN, B=OPEN
W3B			T=OPEN, B=OPEN	T=OPEN, B=OPEN	T=CLOSED, B=OPEN
W23A	SIDINGS	SOUTH-WEST	T=OPEN, B=OPEN	T=OPEN, B=OPEN	T=OPEN, B=OPEN
W23B			T=OPEN, B=OPEN	T=OPEN, B=OPEN	T=CLOSED, B=OPEN

Table 1: Parameter variations within the eight test walls (T=top opening, B= bottom opening, OHJ= open head joint).

2.3. Measuring methods

In total four measuring methods have been applied to study the ventilation rate behind the abovementioned cladding systems: 1) tracer gas, 2) hot bead anemometry, 3) pressure differential sensors and 4) temperature combined with humidity sensors. The applicability and accuracy have been extensively studied and are documented in [16]. The tracer gas method appeared to be influenced by the density of the tracer gas which impeded performing continuous registration of the air change rate. The temperature and humidity method proposed in [16] is limited to the estimation of the order of magnitude of the air change rate due the assumption in this method. In addition this method was limited to rainy periods and is only applicable for moisture buffering claddings systems (e.g. brick veneer). In summary [16] concludes that the highest accuracy was reached with the hot bead anemometry and pressure differential measurements. The study showed a good agreement between the two measuring methods for ventilation rates behind sidings. Yet the study concluded that the ventilation rate behind brick veneer could only be measured with the pressure sensors. The ventilation rate behind brick veneer cladding is typically very low which causes high uncertainty on the data obtained with anemometry. In the present paper only the data generated by the hot bead anemometry and the pressure measurements will be used. These measuring methods will be briefly outlined below. Further information on the measuring methods can be found in [16].

2.3.1. Hot bead Anemometry

The test walls with sidings are equipped with omnidirectional hot bead anemometers[1], located in the middle of the cavity (see Figure 1). The velocity within the cavity is registered every 10s. For fully-developed laminar flow conditions between parallel surfaces the shape of velocity profile corresponds to a parabolic function, so, the ratio between the maximum velocity (u_{max}) and averaged velocity (u_m) is 0.67 [25]. This straightforward relation does not hold for higher air velocities. Experimental work by Falk [5], however, showed that this ratio lies between 0.61 and 0.69 for air velocities below 1 m/s for similar shaped ventilation cavities. Because this corresponds to a small deviation from a parabolic velocity profile, a ratio between the averaged velocity (u_m) and with maximum velocity (u_{max}) of 2/3 is assumed in the present work:

$$\mathbf{ACH} = \frac{\mathbf{u_{max}.2/3}}{\mathbf{h}}.\mathbf{3600} = \frac{\mathbf{u_m}}{\mathbf{h}}.\mathbf{3600} \quad (1)$$

with h the height of the cavity. The advantage of this method is its prompt and continuous registration of the air change rate. The main disadvantages however are the lower limit of these sensors (u_{max} > 0.05 m/s or ACH > 45 1/h), their independency of the flow direction and the low spatial measuring resolution.

2.3.2. Air pressure measurements

All test walls are provided with three air pressure gauges[2] to measure the air pressure drop across the overall cavity every 10 s (see Figure 1). The measured air pressure differentials are translated to air change rates by modelling the cavity as a hydraulic network. This indirect method is based on the relation between the total air pressure differential $\Delta\mathbf{P_{driv}}$ across the cavity and the resulting airflow (Q) which is most often fitted with a power law function:

$$Q = C\Delta P^n \quad (2)$$

This relationship was determined experimentally and theoretically for both cladding systems and is documented in a previous paper [16]. Table 2 briefly summarizes the properties which will be applied in the remainder of this paper.

cladding	C (ACH/Pa^n)	n (-)
brick veneer		
1 OHJ/m	7.4	0.51
2 OHJ/m	14.8	0.51
sidings	765	0.55

Table 2: Air permeability properties according to Eqn. 2 (based on[16]).

[1] Sensor-Electronic AirDistSys 5000F (accuracy: ±0.02 m/s or 1% of reading, measuring range: 0.05-5 m/s)

[2] Halstrup Walcher P26 and P92 (accuracy: ±2% of reading, range: ±100Pa)

2.3.3. Hygrothermal conditions

In addition to the air change rate measurements, sensors are installed to register the hygrothermal conditions behind the cladding system. Each wall is equipped with a grid of 15 thermocouples[3] and 4 relative humidity sensors[4] according to Figure 1.

3. Driving potentials

Cavity ventilation is driven by pressure differentials which can be caused by: 1) thermal buoyancy and 2) wind pressure distributions. Thermal buoyancy is mainly related to solar radiation and corresponds to upward flow conditions. Wind pressures may however result in either upward or downward air flows depending on the wind conditions and the building configuration. In next sections both potentials will be discussed and verified with experimental data.

3.1. Thermal buoyancy

Thermal buoyancy is driven by temperature differences between the cavity and the outer climate. Following from the ideal gas law the related pressure differential caused by temperature differences across the wall cladding can be expressed by:

$$\Delta p_b = \frac{P_{atm}\, g}{R}\left[\frac{h}{T_{out}} - \int_z \frac{dz}{T_c(z)}\right] \cong 3462\left[\frac{1}{T_{out}} - \frac{1}{T_{cm}}\right].h \qquad (3)$$

in which Δp_b corresponds to the pressure differential related to thermal buoyancy, T_{out} is air temperature of the outdoor climate, $T_c(z)$ is the temperature within the cavity, h is the height of the cavity, P_{atm} is the atmospheric pressure, g the gravity acceleration (9.81 m/s²) and R the gas constant of dry air (287 J/kg/K). In what follows the spatial averaged temperature in the cavity (T_{cm}) is assumed to be the measured temperature in the middle of the cavity. Figure 2 illustrates the air change rate based on measured velocities in the cavity (Eqn. 1) as a function of A) the temperature difference between the middle of the cavity and outer temperature and B) the pressure difference related to thermal buoyancy Δp_b according to equation 3 for wall W23A. This figures covers a period from May to July 2014 and the data points are limited to periods with low wind speeds (w<1 m/s).

[3] Thermo Electric Type TT (accuracy: ±0.1 °C, range -20°C/60°C)

[4] Honeywell HIH-4000/21 (accuracy: ±2% of reading, range: 0-100%)

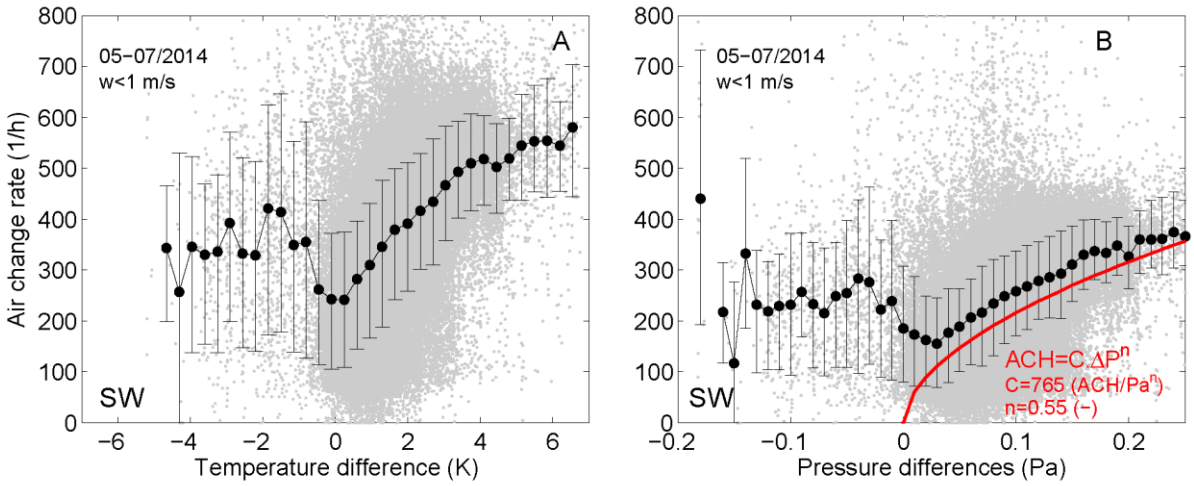

Figure 2: Air change rate behind W23A based on the measured velocity as a function of A) Temperature difference between outer climate and cavity and B) pressure difference based on equation 3. The grey dots represent 10-second data, the black dots correspond to the mean value and the error bars give the 70%-interval. The red curve represents in addition the air flow characterisic of the sidings system adopted from [16]. The data is recorded on the SW oriented test wall and is restriced to periods with low wind velocities (w<1m/s).

Figure 2A shows a distinct power law relation when the cavity's temperatures are greater than the outer temperature. These temperature differences are typically induced by solar radiation. For negative temperature difference, which generally occurs due to undercooling at night, this trend cannot be observed. The reason for the lack of this trend might be the low number of data points with negative temperature differences. Figure B compares the obtained measurements with the theoretical power law relation between the air change rate and the pressure difference (Eqn. 2). The fitting parameters C and n for this relation are adopted from [16] in which these parameters are derived based on a hydraulic network approach for the present cladding configuration. This curve is given in red in Figure 2B and shows a good agreement with the measured air change ranges.

3.2. Wind-induced pressure differential

The wind-induced pressure differences between the top and bottom opening can be derived from Bernoulli's equation [11]:

$$\Delta p_w = \Delta C_p \frac{\rho_a . U_m^2}{2} \tag{4}$$

in which Δp_w is the time-averaged pressure difference due to wind, ΔC_p corresponds to the difference in the local wind pressure coefficient at the top opening and the bottom opening, ρ_a refers to the density of air and U_m is the time-averaged wind speed in the nearby free field. Local wind pressure coefficients (Cp) are influenced by a broad range of parameters (e.g. wind speed and wind direction, building shape, location on the facade, the

degree of exposure). Several authors have studied local wind pressure coefficients for low rise building (e.g. [19,20,21]). A number of analytical models to estimate the local wind pressure coefficient are available in the literature (e.g. Swami & Chandra's model [19] which is adopted by ASHRAE and the Cp-generator developed at TNO [20]). These models are developed based on wind tunnel and/or full scale experiments and aim to provide a prediction for common building shapes. The models are typically constructed based on long averaging periods which may overrule dynamic wind effects. Accordingly, most of the wind tunnel tests have been performed under steady state conditions. For quasi-steady state conditions, the highest difference in the local wind pressure coefficients are obtained along the windward side of the building. Under these conditions downward air flow is predicted in the wall cavity. On the leeward side, however, these models predict a ΔC_p close to zero corresponding to very limited air change rates within the ventilation cavity.

In dynamic wind conditions the local wind pressure coefficient may highly deviate from its value under static conditions. A Danish study by Gudum [2] shows great deviations between the measured local wind pressure coefficients at the top and bottom of rainscreen cladding and its predicted values from the static Cp-generator [20]. In addition to these analytical relations for wind pressure coefficients a few authors document wind pressure coefficients based on numerical simulations. Nore et al. [22] for example studied wind-driven ventilation behind siding cladding based on numerical CFD calculations for a low rise building. Herein they derived the local wind pressure coefficient at the top and bottom of the walls cladding from detailed CFD calculations. These coefficients are then applied in a second step in a hydraulic network model to estimate the ventilation rate. In a related study [23] Nore shows a clear relation between ΔC_p and the wind direction; ΔC_p for a wind direction perpendicular to the building of 0.15-0.2 (-), 0.075-0.0125 (-) for angle of 45° and 0.025-0.075 (-) for an angle of 67°. Again it should be noted that these numerical calculation results are for static wind conditions. Falk and Sandin [5], on the other hand, measured local wind coefficients on a similar low-rise test building in Sweden under dynamic wind conditions. They obtained pressure difference coefficients in a range of 0.025 to 0.05 (-). In contrast with the abovementioned methods under static wind conditions or averaged field data over long periods, these authors didn't find a clear correlation between the wind direction and the difference in local wind pressure coefficients at the top and bottom of ventilation cavity.

Figure 3 verifies the applicability of equation 4 for the data obtained in the present study. This figure shows the wind induced pressure differential between the top and bottom ventilation opening on the Southwest façade (W24A) as a function of the recorded wind speed. The buoyancy driven pressure differentials (calculated from Eqn. 3) were subtracted from the measured pressure differentials to obtain the wind induced pressure differentials. A positive pressure differential corresponds to downward air flow. The data in figure 3 is limited to

periods with a wind direction from the South-West (180°-270°). The measuring points are curve fitted with equation 4, indicating an increasing correlation with increasing averaging period. For an averaging time of 10 seconds the coefficient of determination (r^2) is only 0.009 (-). For an averaging period of 10 minutes and 1 hour the ΔC_p found is 0.029 with a coefficient of determination of 0.43 and 0.49 respectively. The order of magnitude of these ΔC_p's are in line with the values documented in [5]. Yet the results in Figure 3 indicate large fluctuations on the time averaged values. In addition this figure provides the probability density function of pressure differential at a wind speed of 1,3,5,7, 9m/s for the 10 secondly averaged data. These graphs reveal an increasing scatter with an increasing wind speed. Averaged over time the overlaying air flow direction in the cavity is downward. Yet these graphs indicate that the air flow direction is highly changing under dynamic wind conditions.

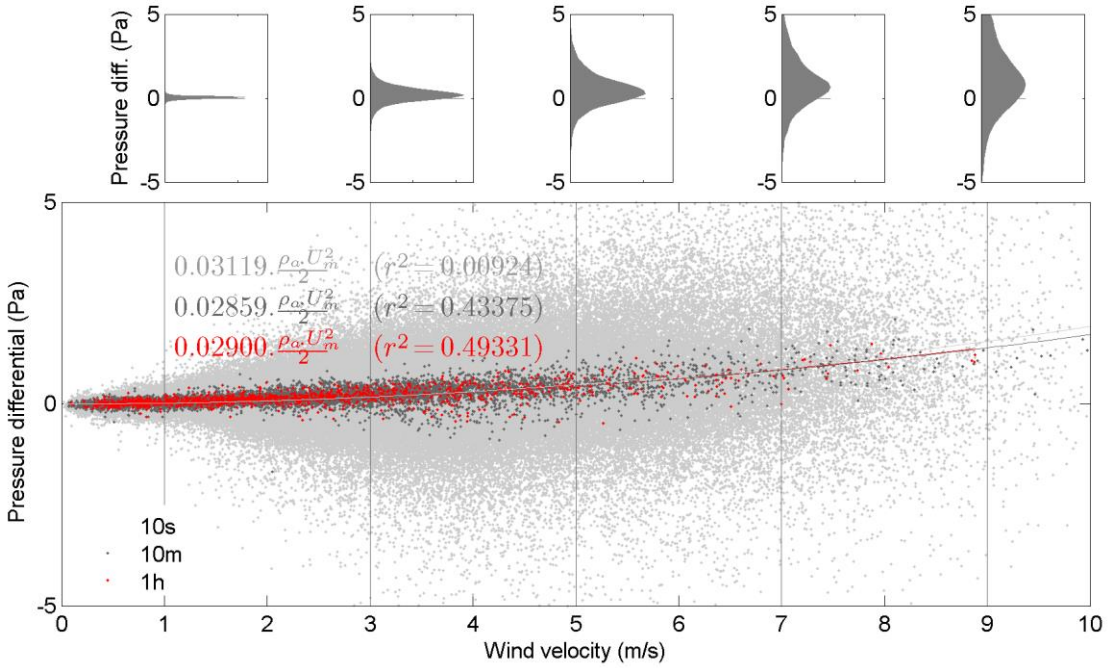

Figure 3: Measured pressure differential across top and bottom ventilation opening as a function wind velocity (10-second averaged data, 10 minute averaged and hourly averaged). Top) Probability density function of pressure differential at a wind speed of 1,3,5,7, 9m/s. (South West orientation (180°-270°), 02-05/2014).

4. Parametric study

This section investigates the impact of 3 design options on the overall cavity ventilation rate. First, the impact of the cladding system is studied. Two rainscreen cladding systems are compared: 1) brick veneer and 2) sidings. Thereafter the impact of the ventilation openings in these systems is investigated followed by the influence of the orientation of the facade. Finally the effects of these parameters on the hygrothermal conditions behind the

cladding will be outlined at the end of the section.

4.1. Cladding system: brick veneer versus sidings

The impact of the cladding system is studied for the South West oriented test walls (W24A/W23A) from March until July 2014. As discussed in section 2 the ventilation openings in claddings systems with sidings are typically larger than the ventilation openings in brick veneer cladding. During this period the top and bottom ventilation openings of the wall with sidings were completely free over the total width of the element and the test wall with brick veneer had 2 open head joints per meter (OHJ/m) at the top and bottom. The cavity ventilation behind the wall with sidings was measured both with anemometry (section 2.3.1) and with pressure gauges (section 2.3.2). The air change rate behind brick however could only be determined with the pressure gauges for the reasons discussed in section 2.3.

Figure 4 plots the cumulative distribution of the air change rates behind brick (red) and sidings (grey/black). The latter is measured both with point anemometry (grey) and pressure gauges (black) showing a good agreement between these two methods. In addition the 15% and 85% percentiles of the ventilation rate are provided in Figure 4. The results illustrate that the air change rate behind the brick veneer is about two orders of magnitude smaller than behind the systems with sidings during this measuring period. It was found that for 70% of the time the level of cavity ventilation behind the brick veneer lies between 3.3 – 11.6 ACH. For the wall with sidings this range was between 151.0 and 592.3 ACH. This indicates that the larger ventilation openings in the walls with sidings result in a significantly higher ventilation rate.

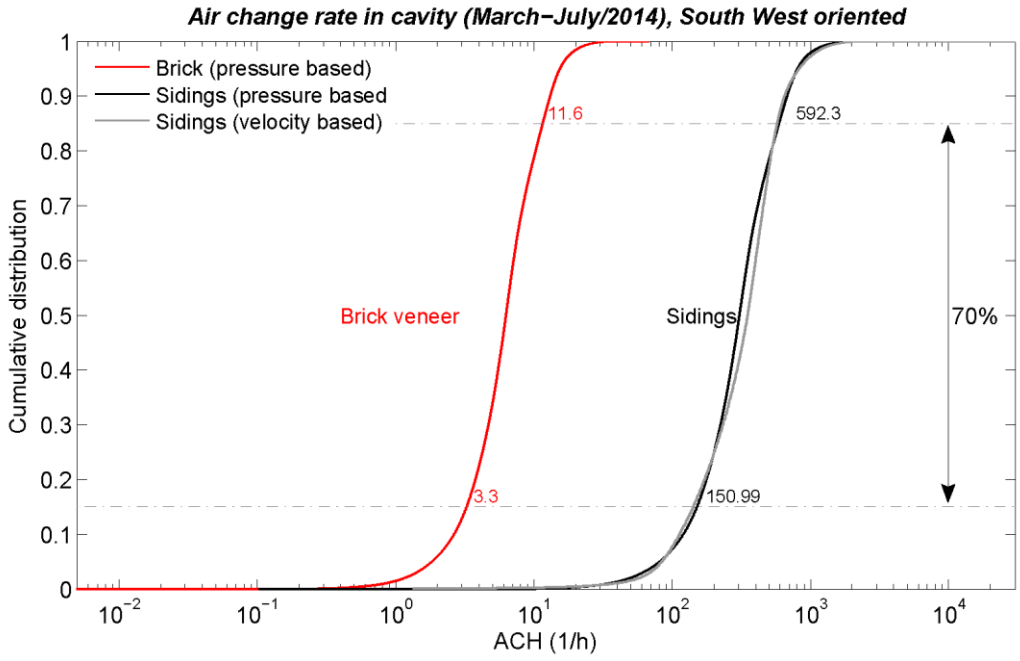

Figure 4: Cumulative distribution function of air change rate behind brick veneer (2 OHJ/m) and sidings based on measured pressure differentials (red/black) and based measured velocity for sidings (grey).

4.2. Number of ventilation openings

The second parameter investigated is the number of ventilation openings. From February to July the impact of different ventilation openings is investigated on the South West façade (W23A/B and W24A/B). Wall 23B was closed at the top while both top and bottom ventilation opening for wall 23A were left free. The brick veneer cladding of W24A had 2 open head joints at the top and bottom and 1 open head joint of top and bottom for wall section W24B. Again the cumulative distribution of air change rate within the test sections is applied to visualize the impact of the ventilation openings. This parameter investigation was conducted in February for the brick veneer walls and from April until July for the walls with sidings. During these periods the two variants were measured under the same meteorological conditions, so, the results are directly comparable. Figure 5 shows that the impact of closing the upper ventilation outlet of the sidings corresponds to a 30 to 36% reduction of the ventilation rate. The reason for this rather limited reduction is related to the fact that sidings are not completely airtight. Though it is not a fully open joint system, still a significant amount of the ventilation is realised through the joints in between the sidings. The air permeability of the sidings of this instance have an air permeance coefficient of 0.004 $m^3/m^2/Pa^{n-1}/s$ and the flow exponent n was 0.59 [16].

The reduction of the open head joints in the brick veneer rainscreen from 2 to 1 joint per meter at both top and bottom results in a 50% decrease of the cavity air change rate. The air flow resistance of the cavity itself is negligible compared to the resistances of the open head joints. Therefore the number of open head joints is the decisive parameter in the global air resistance of the system, and thus, by the extent of the cavity ventilation rate.

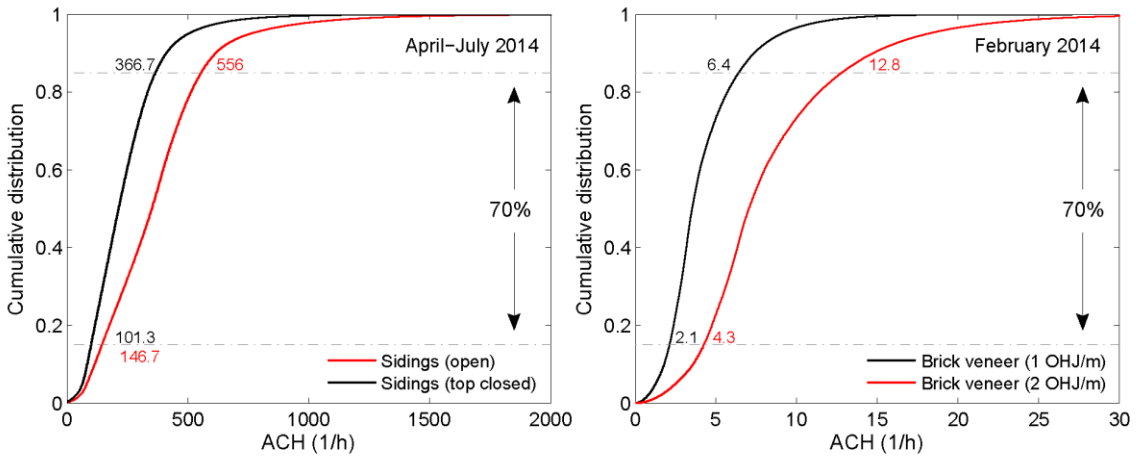

Figure 5: Impact of ventilation openings on the overall air change rate for South West oriented wall with brick veneer and siding cladding.

4.3. Impact of orientation

Section 3.2 mentioned several studies in which local wind pressure coefficients have been investigated [e.g. 19, 20, and 21]. The coefficients in these studies are typically provided as a function of the wind direction. These studies, usually based on static wind conditions or field tests averaged over long periods, predict the greatest differences in Cp between top and bottom of low rise building on the windward side. On the leeward side of the building, however, these models give a rather constant Cp profile which corresponds in theory to no wind driven cavity ventilation.

Figure 6 quantifies the impact of the orientation on the air change rate from March until July. This figure compares the measured air change rates on the North East and South West for brick veneer (W4/24A) and sidings

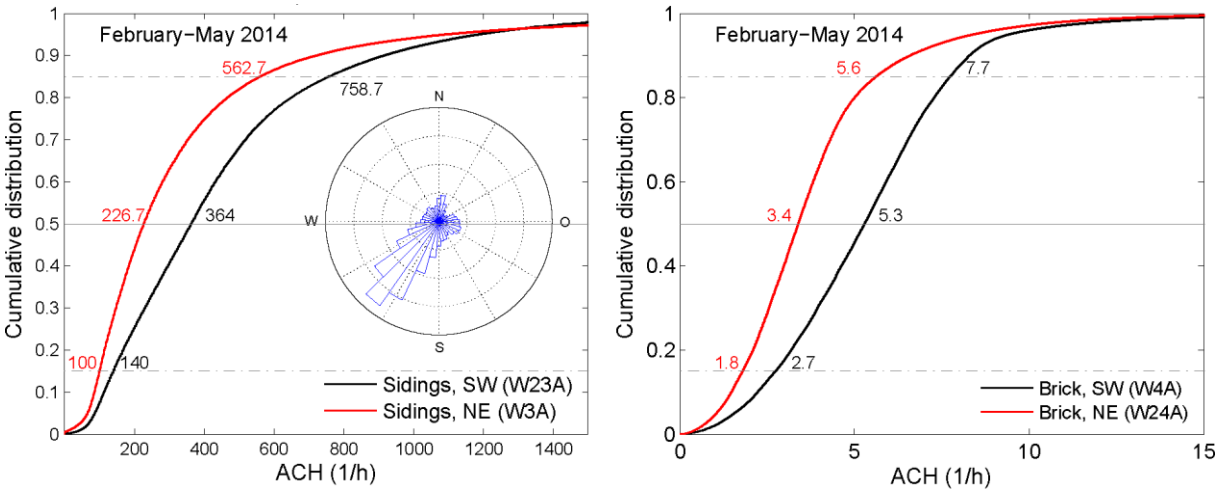

Figure 6: left) Air change rate behind South West and North East oriented sidings and b) Air change rate behind South West and North East oriented brick veneer (March-July 2014).

(W3/23A). The inset of Figure 6 shows a wind rose of the measuring period revealing that the North East façade mainly corresponds to the leeward side and the South West walls to the windward side. The results indicate that for both cladding systems the air change rate on the North East façade is lower than on the South West side. Yet, the reduction is only 25-40%. This difference is much smaller than what would be expected from typical local Cp profiles based on static wind conditions available in the literature [24]. In order to investigate whether this difference is induced by thermal buoyancy or by wind pressure Figure 7 and 8 split out both potentials for cold as well as for warm outside conditions.

Figure 7 investigates the temperature profile within the cavity and compares the pressure difference related to thermal buoyancy with the wind pressure differences on the South West and North East oriented test walls

during a cold period. The left hand side graph depicts the temperature trends for a few days in winter. The right hand side figure includes the cumulative distribution of pressure differential potentials for the month February.

The temperatures on North East oriented walls follow – apart from undercooling effects by night - closely the outdoor temperature. Induced by solar radiation, the temperature on the South West façade can be more than 10°C higher than the outdoor temperature which results in buoyancy driven upward cavity ventilation. This is represented in the right hand side plot in Figure 7 in which the black curve (South West) corresponds to a higher absolute buoyancy induced pressure differential than the red curve (North East). This figure further reveals that the wind driven pressure differential is higher on the South West façade (full blue curve) when it comes to downward flow and higher on the North East side for upward flow (dashed blue line).

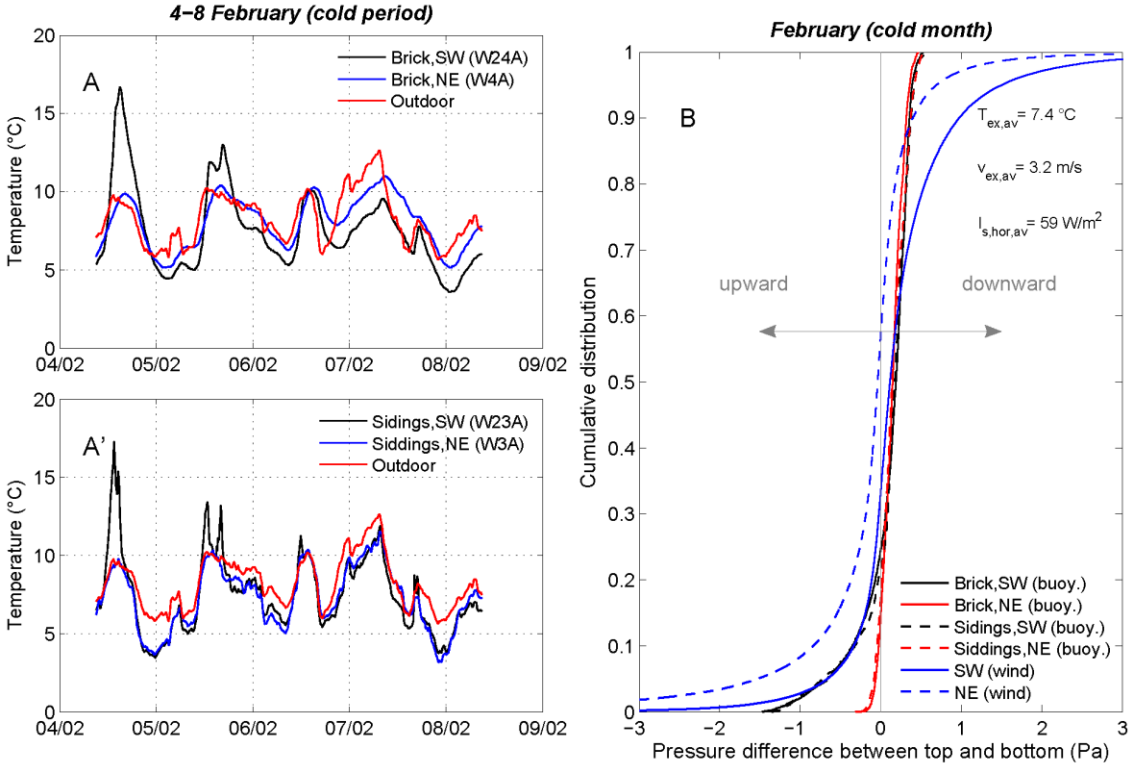

Figure 7: left) Temperature at mid heigt of the cavity for a winter period and right) air pressure differential across the cladding for a cold month (February).

The same graph is plotted in Figure 8 for a warm period. Figure 8a illustrates that due to solar radiation the temperature in the cavity on the South West façade now may be more than 15°C higher than the outer air temperature. This is reflected in Figure 8b in which the black lines correspond to an increased negative pressure differential which corresponds to buoyancy driven pressures. It can be noted in addition that on the North-East oriented walls an increased pressure differential is present due to thermal buoyancy in the morning. The wind induced pressure differentials, on the other hand, show the same profile as Figure 7. Again the highest potentials

for downward flow conditions is established on the South West façade. Yet the level wind induced pressures is lower than in February (Figure 7b) which can be explained by the lower averaged wind speed during this period which is indicated on the top right of the figures.

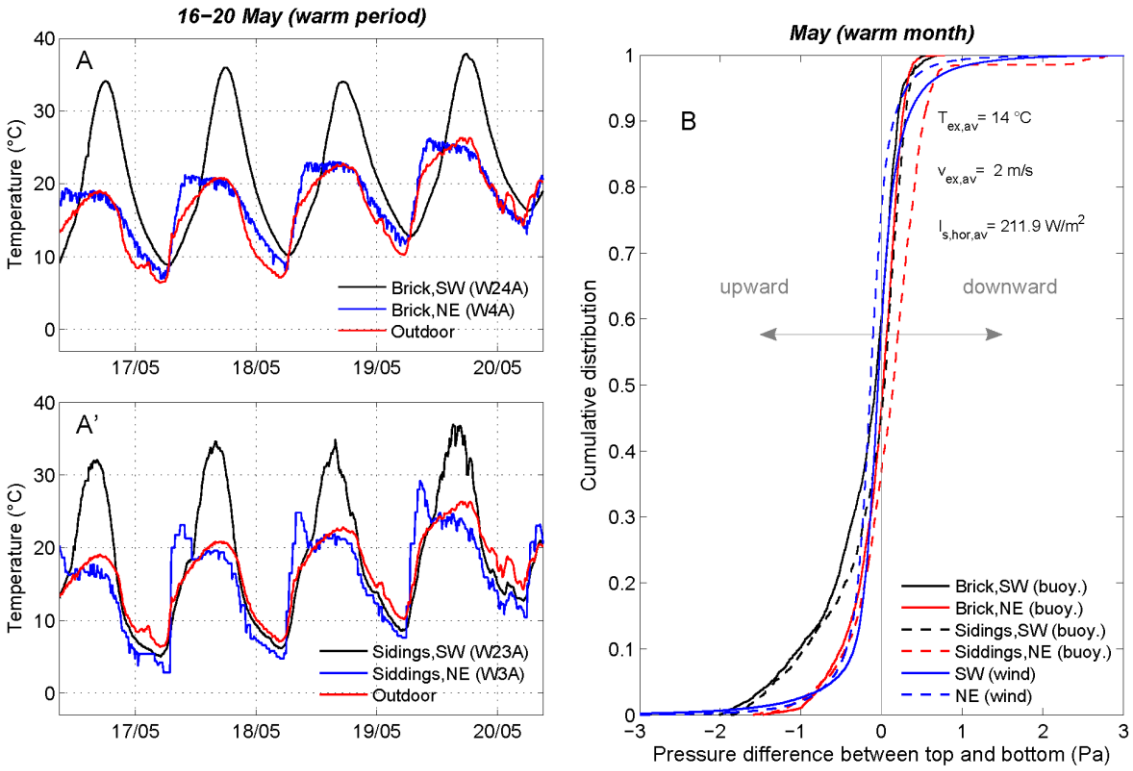

Figure 8: left) Temperature at mid heigt of the cavity for a period in spring and right) air pressure differential across the cladding for a warm month (May).

In summary it can be stated from Figure 7 and 8 that the order of magnitude of the air pressure differential induced by thermal buoyancy and wind are in the same order of magnitude. Figure 7b clearly shows the presence of significant wind induced pressure differentials on the North East façade. This emphases the importance of dynamic wind effect resulting in non-negligible air changes rate on the leeward side.

4.4. Hygrothermal impact of parameters

This section describes the observed hygrothermal conditions in the cavity of the different cladding systems. First the impact on the temperature profile will be discussed followed by the influence of the cladding design on the humidity conditions in the cavity.

4.4.1.Impact on temperature profile in cavity

Figure 9a shows the temperatures profile in the middle of the South West oriented test walls for a week in February. This graph illustrates that the temperature behind the brick veneer is slightly higher than the cavity temperatures behind the sidings when the walls are exposed to solar radiation. This is caused by the interaction

of several physical effects. First, the walls with brick veneer have a lower ventilation rate which means that the cavity will be cooled less due to ventilation of outer air. Second, the solar absorption coefficients of both cladding systems are probably not equal. The solar absorption coefficients have not been measured but based on their colour it can be assumed that the solar adsorption coefficient of the sidings is smaller. In addition, the brick veneer walls have a higher thermal inertia causing a phase shift and a truncation of temperature peaks. The difference in thermal inertia can also be noted on the temperature rise behind the sidings due to a short period of increased solar radiation (e.g. March 1th). In the walls with brick veneer, on the other hand, the solar radiation is absorbed by the outer layer and does not result in a temperature rise in the cavity. The temperature in the brick veneer cools down slower after periods of increased solar radiation due to its difference in heat capacity. As a consequence, the cavity temperature during night is higher for these walls. In addition Figure 9a illustrates that, for both cladding materials, reducing the air change rate has a negligible impact on the cavity temperature. No significant temperature differences are noticed between the walls with different ventilation openings.

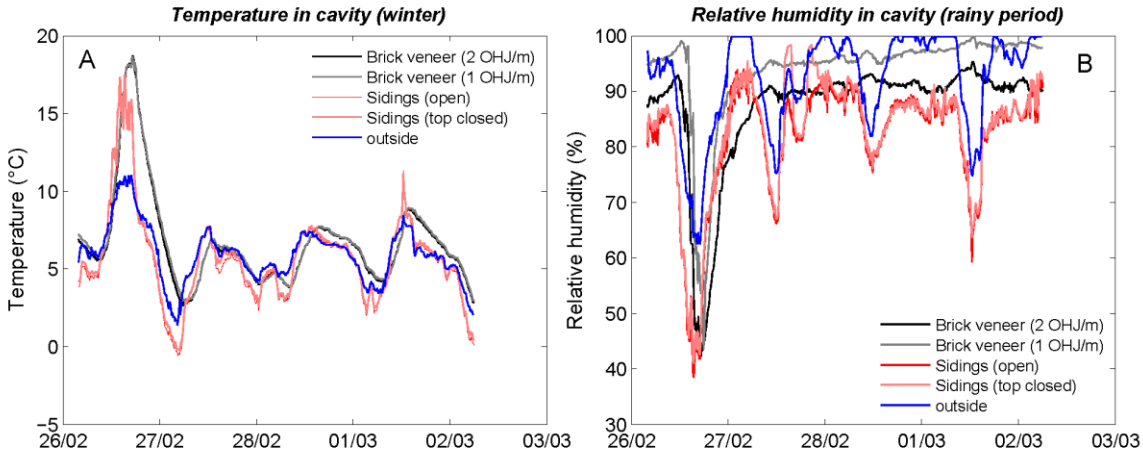

Figure 9: Temperatures and relative humidity readings in the middle of the two cladding systems with various ventilation opening (Southwest oriented test walls).

4.4.2.Impact on humidity conditions in cavity

Figure 9b shows for the same (rainy) period the relative humidity conditions within the four cavities. This figure reveals that the overall humidity conditions behind the sidings are lower compared to the brick veneer cladding during this period. In contrast to the humidity behind the brick veneer, the moisture conditions behind the sidings appear to follow the same trend as the outdoor humidity conditions. This is caused by the higher ventilation rate behind siding rainscreen. The comparison of the two red lines in Figure 9b (W23A/B) shows that the impact of the reduced ventilation rate in the cavity of the sidings has a negligible effect on the recorded relative humidity. Reducing the ventilation rate results only in a minor increase in the humidity (e.g. on 27/02 in Figure 9b) for the

walls with sidings. In contrast, humidity levels were observed behind the brick veneer with only one open head joint per meter (grey curve) compared to the wall with two open head joints (black curve). This indicates that the even low ventilation rate behind brick veneer claddings is essential to dry the cavity. This is further illustrated by Figure 10 in which the humidity conditions are plotted for a longer range (February – July). Herein Figure 10a depicts the wind direction and the cumulative rain precipitation. The periods of frequent rain are in the beginning of February and in May, both corresponding to mainly a South West wind direction. These rainy periods are reflected in high relative humidity levels behind brick veneer on the South West façade in Figure 10b. On March 7th the open head joints in W24B/4B were closed which has a large impact on the drying potential of the South West oriented cladding systems. The cavity behind brick veneer cladding without open head joints (red curve) in Figure 10b remains close to saturation conditions until the end of April. The wall with 2 OHJ/m (blue curve), however, starts to dry in the course of March. The impact of reduced cavity ventilation has far less influence on the humidity conditions on the North East façade (W3A versus W3B). This is because the wind driven rain is limited on this façade orientation.

The humidity conditions behind the walls with sidings on the other hand are hardly influenced by the orientation or the change in ventilation rate. Figure 10c illustrates that the relative humidity behind the sidings is fluctuating more than behind brick. Because of the high ventilation rate The conditions behind the sidings are directly influenced by the outdoor conditions due to the high ventilation rate in these cavities.

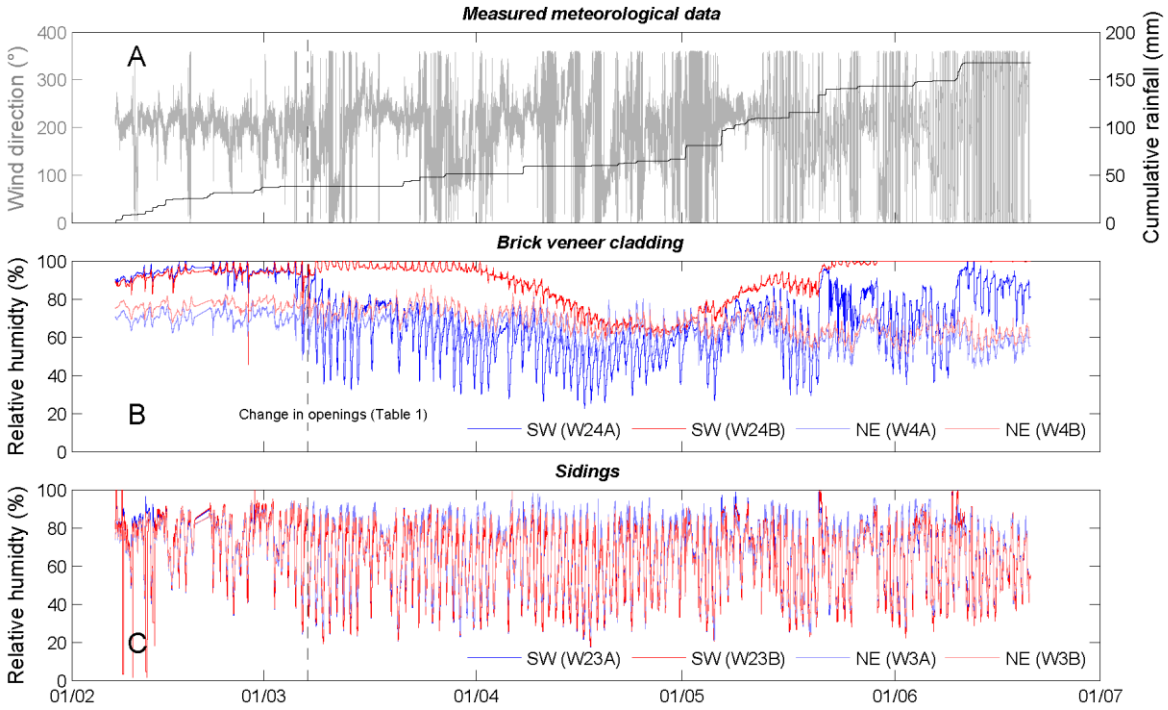

Figure 10: a) Wind direction and cumulative rain precipication nearby the test walls b) relative humidity conditions in the middel of the cavity (brick) and c) relative humidity conditions in the middle of the cavity (sidings).

5. Implications and recommendations for numerical HAM-modelling

The introduction section mentioned the different alternatives on how to implement cavity ventilation in common Heat, Air and Moisture (HAM) models for building components. Figures 9 and 10 illustrated the large differences in the hygrothermal conditions within the cavity for two different cladding materials. As a consequence, the degree of accuracy of the ventilation model needed is related to the applied cladding system. In what follows the generated field data will be applied to provide recommendations to include the ventilated rainscreen cladding systems of this instance in building component HAM-models.

Figure 11 compares the outdoor vapour pressure with the vapour conditions behind both brick veneer (black dots, W24/4A) and sidings (red dots, W23/3A) for the two orientations investigated.

Figure 11 reveals that for both orientations the vapour pressure behind brick veneer (black dots) is significantly higher than the outdoor vapour pressure. Especially on the South West façade a pronounced increase can be noticed. This is related to a combination of a low ventilation rate within these cavities (see Figure 4) and the moisture buffering capacity of the brick layer. This implies that in order to produce realistic hygrothermal simulations for walls with brick veneer cladding it is highly important to include in the model the coupled heat and moisture transport in the brick layer in interaction with air flow.

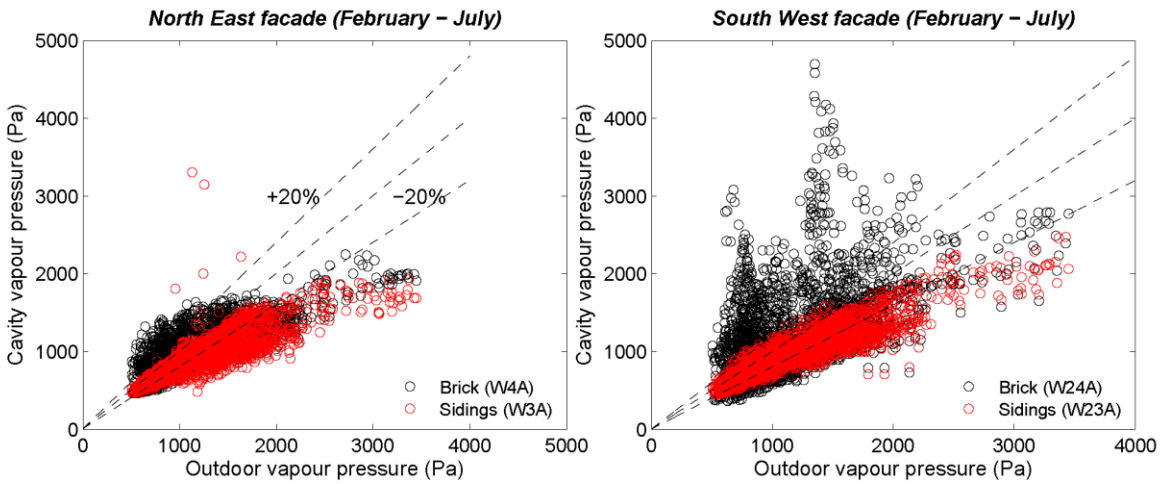

Figure 11: Comparison of vapour pressure in cavity with outdoor vapour pressure for a) North East and b) South West oriented brick veneer and siding cladding (hourly averaged).

In contrast, the graphs in Figure 11 further illustrate that the vapour pressures behind the sidings are lower than the outdoor vapour pressure for both orientations. Based on this figure it can be stated that - when it comes to humidity related boundary conditions – it is a safe assumption to impose the outdoor vapour pressure directly and exclude the cladding layer and its ventilated air layer from the model for sidings rainscreen.

Yet excluding this layer implies the need to compensate for temperature differences related to radiation. This is further investigated in Figure 12. This figure compares similar to Figure 11 the outdoor air temperature with the temperature in the cavity for both orientations. This figure reveals that the differences between both temperatures are limited on the North East orientation. On the South West façade however the difference increases due to solar radiation. For this orientation the HAM-model should be adjusted to capture the temperature increase due to solar radiation in case the cavity is excluded from the model.

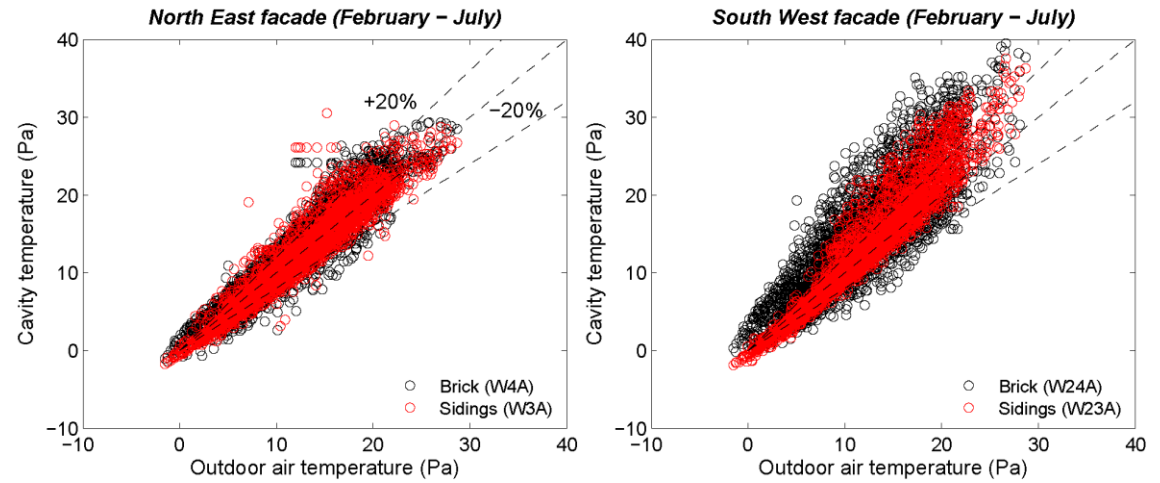

Figure 12: Comparison of tempeature in cavity with outdoor air temperature for a) North East and b) South West oriented brick veneer and siding cladding (hourly averaged).

In summary it can be stated from Figure 11 and 12 that a detailed model capturing the interaction between the moisture buffering brick veneer cladding and the cavity is essential for a detailed HAM-simulations including brick veneer . On the other hand, for siding systems, it is a safe assumption to impose the outer vapour pressure directly. Yet Figure 12b illustrates the necessity to account for increased surface temperatures due to solar radiation on the South West façade.

6. Discussion and conclusions

The type of rainscreen cladding and the relating design options may influence the effectiveness of cavity ventilation in wall elements. Yet due to the dynamic nature of the air flow processes behind cladding systems, still significant uncertainties exist in the literature when it comes to a quantitative description of the ventilation rate. In addition little recommendations on how to implement cavity ventilation correctly in HAM-models are currently available.

This article presents the results of a large-scale experiment to investigate the impact of several design options on the overall air change rate behind rainscreen cladding. In total 8 full-scale test walls have been studied in field conditions. The parameter study includes a variation in a) the type of cladding, b) area of ventilation openings and c) the orientation.

The results reveal that the ventilation rate behind sidings with top and bottom ventilation openings (100-1000 ACH) is about two orders of magnitude higher than the ventilation rate behind brick veneer with 1 open head joint per meter (1-10ACH).

The study further illustrates that closing the upper ventilation opening in a system with sidings reduces the overall ventilation rate by 30-36 %. For the brick veneer rainscreen, on the other hand, reducing the number of ventilation openings from 2 to 1 open head joint per meter corresponded to a 50% reduction of the overall ventilation.

The paper shows that the ventilation rate on the leeward side of the building is only 25 to 40% lower than on the windward side. This, while static wind pressure tests predict an almost constant Cp profile along the height of the building on the leeward side corresponding to very low ventilation rates. The measurements of this instance illustrate that the ventilation rate on the leeward side is significantly higher due to dynamic wind loads. Similar findings have been published by Falk et al. [5] in which the authors state that they did not find a clear correlation between the wind direction and the differences in local wind pressure coefficients at the top and bottom of ventilation cavity.

In addition to the quantification of the ventilation rate the present article verified the impact of the cladding systems on the hygrothermal conditions within the cavity. The results indicate that the impact of the number of ventilation openings hardly influenced the temperature behind both cladding systems. For the humidity conditions on the other hand, an impact of the ventilation openings on the relative humidity was noticed. Especially for the walls with brick veneer on the South West façade a lower ventilation rate corresponded to higher humidity conditions behind the cladding. The measuring data emphases the importance of providing a minimum of ventilation openings within brick rainscreen cladding on the South West façade. Absence of sufficient ventilation behind this system will result in long periods with almost saturated vapour conditions. Combined with timber frame elements behind such unventilated brick veneer cladding might result in ideal conditions for mould growth.

Finally the generated field data is applied to suggest recommendation for the implementation of cavity ventilation in building component HAM-models. The results indicate that highly ventilated rainscreen cladding, such as sidings, can be excluded from the numerical model. Yet in such cases it is still important to compensate for a temperature increase due to solar radiation. When it comes to poorly ventilated systems, such as brick veneer, excluding the cladding layer within the HAM-model will result to an underestimation of the hygrothermal loads. For these systems it is essential to include the cladding layer in the model to capture the moisture transport within this layer in interaction with the air flow in the cavity. First attempts on the implementation of such models have been published recently by Van Belleghem et al. [19]. Though this model is very promising its major drawback is the current long calculation time impeding its use for yearly simulations.

Acknowledgements

Research funded by a Postdoctoral Innovation Mandate (grant number 140695) of the Institute for the Promotion of Innovation through Science and Technology in Flanders (IWT-Vlaanderen) and by a research project FWO G.0982.14 of the Research Foundation Flanders.

References

[1] Straube J. High performance enclosures. 1th ed. Waterloo: Building Science Press. 2012
[2] Gudum, C. Moisture Transport and Convection in Building Envelopes. Department of Civil Engineering, Technical University of Denmark. PhD thesis; 2003, see also http://www.byg.dtu.dk/-/media/Institutter/Byg/publikationer/PhD/byg_r047.ashx?la=da
[3] Bassett, M., & McNeil, S. Ventilation measured in the wall cavities of high moisture risk buildings. Journal of Building Physics, 2009; 32(4); 291–303.
[4] TenWolde, A., Carll, C. and Malinauskas, V. Airflows and Moisture Conditions in Walls of Manufactured Homes, ASTM. STP 1255: Airflow Performance of Building Envelopes, Components and Systems, American Society for Testing and Materials, Philadelphia; 2009.
[5] Falk, J., & Sandin, K. Ventilated rainscreen cladding : Measurements of cavity air velocities , estimation of air change rates and evaluation of driving forces. Building and Environment,2003; 59; 164–176.

[6] Labat, M., Garnier, G., Woloszyn, M., Roux, J.J., Infrared measurements on a ventilated cladding for assessing its surface temperature and heat transfer calculation through the insulated part of the envelope using a simulation tool. In: 9th Nordic Symposium on Building Physics, 2011;1;315–322.
[7] Sandin K. Skalmurskonstruktionens fuktoch temperaturbetingelser, R43, Technical University College, Lund; 1991 [in Swedish]
[8] Karagiozis, A., & Künzel, H. The Effect of Air Cavity Convection on the Wetting and Drying Behavior of Wood-Frame Walls Using a Multi-Physics Approach. Journal of ASTM International, 2009; 6(10)
[9] Tenwolde, A., & Carll, C. Effect of cavity ventilation on moisture in walls and roofs. In Thermal Performance of the Exterior Envelope of Buildings VI Conference. Clearwater, USA; 1992
[10] Straube, J., & Burnett, E. Building science for building enclosures. Building Science Press 2005, See also, www.buildingscience.com
[11] Janssens, A., & Hens, H. Interstitial condensation due to air Leakage: a sensitivity analysis. Journal of Thermal Envelope and Building Science, 2003; 27(1), 15–29.
[12] Künzel, H. M., Karagiozis, A. N., & Kehrer, M. Assessing the benefits of cavity ventilation by hygrothermal simulation. In R. S. & V. G. (Eds.), Building physics symposium in honour of Prof.Hugo L.S.C Hens. Leuven, Belgium, 2008
[13] Janssens, A. Reliable control of interstitial condensation in lightweight roof systems: calculation and assessemnt methods. Catholic University of Leuven, Belgium.PhD thesis, 1998 ,see also http://bwk.kuleuven.be/bwf/PhDs/PhDJanssens)
[14] Langmans, J. Feasibility of exterior air barriers in light weight construction. PhD thesis. KU Leuven, 2013, see also http://bwk.kuleuven.be/bwf/PhDs/PhDLangmans
[15] Van Belleghem M., Steeman M., Janssens A., De Paepe M., Heat, air and moisture transport modelling in ventilated cavity walls.Journal of Building Physics, 2015; 38(4); 317-349
[16] Langmans J. and Roels S., (2015) Experimental analysis of cavity ventilation behind rainscreen cladding systems: a comparison of measuring techniques, Building and Environment, 2015; 87(5); 177-192.
[17] Desta, T. Z., Langmans, J., & Roels, S. Experimental data set for validation of heat, air and moisture transport models of building envelopes. Building and Environment,2011;46(5);1038–1046.
[18] Blocken B, Carmeliet J High-resolution wind-driven-rain measurements on a low-rise building - experimental data for model development and model validation. Journal of Wind Engineering and Industrial Aerodynamics 2005;93(12);905-928.
[19] Swami MV, Chandra S. Correlations for pressure distribution on buildings and calculation of natural-ventilation airflow.ASHRAE Transactions1988;94:243–66.
[20] B. Knoll, J.C. Phaff,W.F. de Gids, Pressure simulation program, Proceedings of the Conference 22th on Implementing the Results of Ventilation Research, AIVC, 1995.
[21] Cóstola, D., Blocken, B., & Hensen, J. L. M. Overview of pressure coefficient data in building energy simulation and airflow network programs. Building and Environment, 2009; 44(10); 2027–2036.
[22] Nore, K., Blocken, B., & Thue, J. V. On CFD simulation of wind-induced airflow in narrow ventilated facade cavities: Coupled and decoupled simulations and modelling limitations. Building and Environment, 2009; 45(8); 1834–1846.
[23] Nore, K. Hygrothermal performance of ventilated wooden cladding. Building. Norwegian University of science and technology, Norway. PhD thesis, 2009, see also https://www.ntnu.no/c/document_library/get_file?uuid=3722fd33-c9fa-4762-9bf1-653d627236cd&groupId=10380
[24] Cóstola, D., Blocken, B., Ohba, M., & Hensen, J. L. M. Uncertainty in airflow rate calculations due to the use of surface-averaged pressure coefficients. Energy and Buildings, 2010; 42(6); 881–888.
[25] Bejan, A. (2004). Convection heat transfer (Vol. Third). John Wiley & Sons, New Jersey, USA.